IEEE Access
Multidisciplinary | Rapid Review | Open Access Journal

Received July 21, 2018, accepted July 27, 2018, date of publication September 4, 2018, date of current version September 28, 2018.

Digital Object Identifier 10.1109/ACCESS.2018.2863719

Active Contour Model Based on Local Intensity Fitting Energy for Image Segmentation and Bias Estimation

XIAOYING SHAN[1,2], XIAOLIANG GONG[3], AND ASOKE K. NANDI[3,4], (Fellow, IEEE)

[1]College of Electronic and Information Engineering, Tongji University, Shanghai 201804, China
[2]Normal College, Jiaxing University, Jiaxing 314001, China
[3]Key Laboratory of Embedded System and Service Computing, College of Electronic and Information Engineering, Tongji University, Shanghai 201804, China
[4]Department of Electronic and Computer Engineering, Brunel University London, Uxbridge UB8 3PH, U.K.

Corresponding author: Xiaoying Shan (1510481@tongji.edu.cn)

This work was supported by the Shanghai Natural Science Foundation of China under Grant 16JC1401300.

ABSTRACT Intensity nonuniformity is one of the common issues in image segmentation, which is caused by technical limitations or external interference. In this paper, a novel region-based active contour model is presented for interleaved segmentation of images with intensity nonuniformity and correction of the bias field. First, we define the local region-based fitting image by using the information of bias field and the intensity, and simultaneously introducing the local difference between the input image and estimated image. Next, a likelihood fitting image energy functional is built in a local region around each point. Then, a level set method is used to present a total energy functional, which contains the level set distance regularization term and the length regularization term. Extensive experiments are conducted on synthetic images and real medical images to demonstrate the advantages of our model over the state-of-the-art methods. Segmentation results show robustness to initialization and noise, as well as significant improvements in both accuracy and execution time.

INDEX TERMS Active contour model, bias field correction, image segmentation, intensity nonuniformity.

I. INTRODUCTION

Image segmentation is one of the most basic and important stage in digital image processing and computer vision. In the past few decades, it has been widely researched, and a lot of approaches for image segmentation have appeared [1]–[5]. However, due to complex background, noise and intensity nonuniformity, image segmentation is still a challenging task. Intensity nonuniformity or bias field [6]–[8] caused by imperfections of imaging devices and other external effects often occurs in real images. Because bias field result in the intensity overlaps of object and background, it is hard to get accurate segmentation results.

Active contour models [9]–[12] have been testified to be the efficient methods in virtue of their good properties which can supply segmentation results with a smooth and closed contours and manage with the changes in topology through the use of implicit description of curve evolution described by level set function According to the type of information used, active contour models are roughly grouped into two major categories: edge-based models [18]–[22] and region-based models [13]–[17]. Edge-based models usually construct a gradient stop function to make the contour curve move towards the object edge. Because the intensity gradient information is sensitive to noise, edge-based models are sensitive to image noise and may cause boundary leakage around weak boundaries. Region-based models segment an image by designing a certain region descriptor based on statistical information of inner and outer regions of active contour curve to guide the contour curve evolution. Due to the region descriptor, which is helpful to overcome the limitations of edge-based models to some extent, region-based models are less sensitive to noise and can efficiently segment objects with weak boundaries.

Chan-Vese (CV) model [9] is one of the most representative model in region-based models and it utilizes the average intensities in inner and outer regions of the evolution curve to approximate the image intensities inside and outside the evolution curve, respectively. In other word, a piecewise constant function is employed to search for an optimal approximation of the input image in CV model under the assumption that the object is homogenous and so is background However, this hypothesis is not valid for heterogeneous images, CV model

cannot deal with intensity nonuniformity, which show itself as a smooth intensity variation across the image. To overcome this difficulty, local region-based models [23], [26] are proposed by using intensity information in local regions instead of global intensity information inside and outside active contour. It is generally assumed that images with intensity nonuniformity are homogeneous in local areas around each pixel in these local region-based models Li *et al.* [16], [17] presented a local binary fitting (LBF) model which puts forward an approximation of image intensities in spatially varying local regions The approximation is achieved by using local intensity to construct two fitting functions on both sides of the evolution curve. Ding *et al.* [35] proposed an active contours based on local pre-fitting energy. This model is robust to the initializations and takes less time duo to the fitting functions which are calculated before the evolution of curve. However, the segmentation accuracy may be reduced for some images due to the local pre-fitting functions. Zhang *et al.* [15] presented an intensity fitting energy by minimizing the difference between the input image and the fitting image By using the local intensity information to define the fitting image, it can get promising segmentation results. Wang *et al.* [34] propose a novel image fitting model by defining the square fitted image to approximate the square of the input image. Wang *et al.* [34] also pointed out that this model cannot effectively highlight desirable objects located in images with vague boundaries. Inspired by bilateral filtering, Niu *et al.* [28] utilized local spatial distance and intensity to define a local similarity factor. This model can detect object from images in presence of strong noise and intensity nonuniformity However, the above models do not have the ability for bias correction which is an important assignment for medical image processing.

In order to yield segmentation and nonuniformity correction simultaneously Li *et al.* [23] presented a local intensity clustering (LIC) model by applying K-means method and minimizing the differences between the input image and the local clustering center in the neighborhood around each point. Huang and Li [29] presented a modified local intensity clustering (MLIC) model, which introduced the difference matrix between the input image and estimated image to improve LIC. Zhang *et al.* [25] developed a local statistical model (LSM). In this model, Gaussian distributions was introduced to model the inhomogeneous objects, and a mapping from the input image intensity to local intensity mean was described to suppress intensity nonuniformity However it regularizes the level set function by using Gaussian smooth processing, so it may suffer from the segmentation of undesirable background regions. Li *et al.* [30] developed a new method named multiplicative intrinsic component optimization (MICO) for interleaved segmentation of magnetic resonance (MR) images and estimation of the bias field A linear expression of twenty orthogonal Legendre polynomial functions is utilized to approximate the bias field whose smoothly varying character is guaranteed by the Legendre polynomial functions The experimental results demonstrate that the intensity nonuniformity in the input image and the estimated bias field are consistent However, this model is sensitive to noise. The above models manifested themselves in dealing with inhomogeneous images, but the constructed fitting functions or the cluster centers may be insufficient to mitigate the effects of intensity nonuniformity for certain images and cannot distinguish desirable objects from background. Hence, it is desirable to propose novel segmentation method that can effectively mitigate the effects of intensity nonuniformity.

In this work, we present a novel region-based active contour model for segmentation and bias correction. Based on an image model combining the bias-free image intensity, the bias field and the local difference we construct two local intensity fitting functions that are close to the input image intensities on the two sides of the curve in a neighborhood of every pixel. Afterwards, at each pixel, we formulate a local region-based fitting image in term of the evolution curve and the two aforementioned local intensity fitting functions. A local energy functional is defined by minimizing the differences between the local region-based fitting image and the input image. Then a global energy functional is obtained by combining the local energy functional in regard to neighborhood center in the whole image area. Finally, this global energy is incorporated with an arc length term of the curve and a level set function regularization term that ensure accurate calculation of the level set evolution and avoid expensive re-initialization procedures. Segmentation and nonuniformity correction can be simultaneously implemented by iteratively updating the variables until it is stable or up to the specified number of iterations. The proposed model have been tested on synthetic images and real images. Compared with the state-of-the-art methods, segmentation results show robustness to initialization and noise, as well as improvements in both accuracy and execution time.

The remaining part of this paper is organized as follows. We briefly review some algorithms in section II, our proposed method is introduced in section III In section IV, experimental results and discussions are presented. Conclusions are summarized in Section V

II. RELATED WORKS

A. THE LBF MODEL

Li *et al.* [16], [17] developed the LBF model to overcome the difficulty resulted from intensity nonuniformity. Given an image $u : \Omega \subset R^2 \rightarrow R$, let $\phi(x) : \Omega \rightarrow R$ be a level set function defined on the image area Ω. The evolving curve S can be expressed by the level set function $\phi(x)$ as $\mathcal{S} = \{x \in \Omega \,|\phi(x) = 0\}$, which separates Ω into two areas:$\Omega_1 = inside(S) = \{x \in \Omega \,|\phi(x) < 0\}$ and $\Omega_2 = outside(S) = \{x \in \Omega |\, \phi(x) > 0\}$. For a given pixel $y \in \Omega$, the local energy functional is given by:

$$\varepsilon_y(S, f_1(y), f_2(y)) = \sum_{i=1}^{2} \lambda_i \int_{\Omega_i} K(x-y)\,|u(x) - f_i(y)|^2\,\mathrm{d}x \tag{1}$$

Algorithm 1 The Proposed Model

Input: The original image $u(x)$ and the parametersσ, ε, Δt, μ, and ν.

1: **If** method = two –phase **then**

2: Initialize the level set function ϕ as follows

$$\phi(x) = \begin{cases} -c_0 & x\text{is inside S}, \\ c_0 & x\text{is outside S}, \end{cases}$$

where c_0 is a constant;

3: Initialize the bias field B and local difference v;

4: **while** contour evolution is not converged or the fixed iterative times is not reached **do**

5: Calculate c, B and v from (18)-(20);

6: Update the level set function ϕ based on (17);

7: **End while**

8: **else** (method = three –phase)

9: Initialize the level set function Φ;

10: Initialize the bias field B and local difference v;

11: **while** contour evolution is not converged or the fixed iterative times is not reached do

12: Calculate c, B and v from (29)-(31);

13: Compute γ_1 and γ_2 from (28);

14: Update the level set function ϕ_i based on (26-27);

15: **End while**

16: **End if**

Output: The level set function ϕ, bias field B, the recovered true image c, local difference v.

with λ_1 and λ_2 being fixed positive coefficients; $K(x-y)$ being a Gaussian kernel function; $f_1(y)$ and $f_2(y)$ being two fitting functions that is optimally close to the local intensity value in Ω_1 and Ω_2 When the contour S is precisely located on the boundary of the object. To find the object boundaries, i.e., a curve S that minimizes the local energy ε_y for all y in Ω, the integral of ε_y over Ω is minimized. Therefore, the total fitting energy is formulated by:

$$\begin{aligned} &F(\phi, f_1, f_2) \\ &= \int_\Omega \left(\sum_{i=1}^{2} \lambda_i \int_{\Omega_i} K(x-y) \left| u(x) - f_i(y) \right|^2 M_i(\phi(x)) \mathrm{d}x \right) \mathrm{d}y \\ &\quad + \nu \mathcal{L}(\phi) + \mu \Re(\phi) \end{aligned} \tag{2}$$

where μ and ν are positive constant coefficients; $M_1(\phi(x)) = H(\phi(x))$ and $M_2(\phi(x)) = 1 - H(\phi(x))$ are the membership functions of Ω_1 and Ω_2 with H being the Heaviside function; $\mathcal{L}(\phi)$ and $\Re(\phi)$ are the regularization terms. Traditionally, the first term on the right-hand side of (2) is called as a fidelity term. The distance regularization term $\Re(\phi) = \int_\Omega \frac{1}{2} \left(|\nabla \phi(x)| - 1 \right)^2 \mathrm{d}x$, which was developed by literature [18], is adopted in LBF model to avoid re-initialization of the level set function ϕ which should be a signed distance function in the process of curve evolution. So the distance regularization term can preserve the stability of the level set evolution and achieve accurate calculation. The length regularization term $\mathcal{L}(\phi) = \int_\Omega |\nabla H(\phi(x))| \, \mathrm{d}x$, which measures the length of the zero level set, can smooth the zero level contour and avert small and isolated areas in the segmentation results.

The LBF model can segment nonuniformity images accurately, but if the initial curve position is inappropriate, it easily falls into a local minimum, which means that this model requires strict initial contour position as pointed by literature [27] and literature [31]. Besides, this model has no ability to make correction of the intensity nonuniformity.

B. THE LIC MODEL

In order to yield segmentation and nonuniformity correction simultaneously, the local intensity clustering (LIC) model is presented in [23]. The LIC model is built on the following widely accepted image model

$$u(x) = B(x)J(x) + N(x) \tag{3}$$

with J being the recovered true image, which takes different constant values c_k in each disjoint areas Ω_k, with $\{\Omega_k\}_{k=1}^N$ forming a partition of Ω, i.e., $\Omega = \bigcup_{k=1}^{N} \Omega_k$, and $\Omega_j \cap \Omega_k = 0$ for $j \neq k$; B being the bias field, which is presumed to change smoothly and slowly; and N being the additive noise. The LIC model takes $B(y)J(y)$ as the clustering center approximately in the local area O_y of each pixel y. By applying the K-means clustering algorithm and considering that the pixels in O_y can be classified into N clusters, a local energy function is presented as follows:

$$\varepsilon_y(S, B, c) = \sum_{i=1}^{N} \lambda_i \int_{\Omega_i} K(x-y) \left| u(x) - B(y)c_i \right|^2 \mathrm{d}x \tag{4}$$

where K is a Gaussian kernel function which satisfies $K(x-y) = 0$ for $x \notin O_y$. When the value of ε_y reaches the minimum, the clustering result is the best. To obtain the object boundaries, i.e., a curve S that can minimize the energy ε_y for all y in Ω, the total energy functional can be given by:

$$\begin{aligned} &F(\phi, B, c) \\ &= \int_\Omega \left(\sum_{i=1}^{N} \lambda_i \int_{\Omega_i} K(x-y) \left| u(x) - B(y)c_i \right|^2 M_i(\phi(x)) \mathrm{d}x \right) \mathrm{d}y \\ &\quad + \nu \mathcal{L}(\phi) + \mu \Re(\phi) \end{aligned} \tag{5}$$

with μ and ν being positive constant coefficients; $M_i(\phi(x))$ being the membership functions of Ω_i; $\mathcal{L}(\phi)$ being the distance regularization term and $\Re(\phi)$ being the length regularization term.

Owing to the multiplicative image model of intensity nonuniformity, the bias field and intensity information are taken into account in the LIC model. Therefore, it has capability for image segmentation and simultaneous correction of the bias field. However, employing only the local intensity and bias information is inadequate to fit the input image as has been discussed in the literature [29] and this model still suffers from the defect in sensitivity to the initialization and easily falls into a local minimum.

III. OUR MODEL

A. IMAGE MODEL

The image model employed to depict intensity nonuniformity is given by (3). Many publications have used it for nonuniformity correction. However, employing only the local intensity and bias information is insufficient to estimate the input image, as pointed by Huang and Li [29]. For the sake of more accurate segmentation result, Huang and Li [29] propose an improved image model, which can be formulated as:

$$u(x) = B(x)J(x) + v(x) + N(x) \tag{6}$$

with J being the recovered true image, $v(x)$ being a smooth function, $N(x)$ being the additive noise, and B being the bias field with slowly and smoothly changing characteristic over the whole image region. In this improved image model, $v(x)$ is taken as the local difference between the input image $u(x)$ and estimated image $B(x)J(x)$.

B. LOCAL REGION-BASED FITTING ENERGY

Based on (6), a new local region-based fitting energy is presented. To be specific, at a given point $x \in \Omega$, we consider a small local region with a radius ρ formulated as:

$$O_x = \{y : |y - x| \le \rho\} \tag{7}$$

$\{O_x \cap \Omega_i\}_{i=1}^N$ represents the partition of the neighborhood O_x induced by the partition of the image $\{\Omega_i\}_{i=1}^N$. Due to the slow change of bias field $B(x)$ and difference function $v(x)$, $B(x)$ and $v(x)$ are close to the values $B(y)$ and $v(y)$ for all $y \in O_x$ respectively. According to the image model (6), the input image intensity $u(y)$ is close to the constant $(B(x)c_i + v(x))$ in each sub-region $O_x \cap \Omega_i$, i.e.

$$\begin{aligned} u(y) &= B(y)c_i + v(y) + N(y) \\ &\approx B(x)c_i + v(x), y \in O_x \cap \Omega_i \end{aligned} \tag{8}$$

with $N(y)$ being the noise. Based on the above analysis, we can regard $(B(x)c_i + v(x))$ as the center of the cluster $\{u(y) : y \in O_x \cap \Omega_i\}$.

For convenience, we denote a vector $c = (c_1, c_2, \cdots, c_N)$. Based on above analyses, we define the local region-based fitting image as follows:

$$u_f(y) = \sum_{i=1}^{N} (B(x)c_i + v(x))\, u_i(y), \quad y \in O_x \tag{9}$$

where $u_i(y)$ is a characteristic function of the region and satisfies

$$u_i(y) = \begin{cases} 1 & y \in \Omega_i \\ 0 & y \notin \Omega_i \end{cases} \tag{10}$$

It can easily be seen that when the difference between the fitting image and the input image reaches the minimum, the clustering result in the local area is the best. Thus, the local energy is presented as follow:

$$\varepsilon_x = \int_{O_x} G(x - y) \left|u(y) - u_f(y)\right|^2 \mathrm{d}y \tag{11}$$

where $G(x - y)$ is a window function with the property of $G(x - y) = 0$ for $y \notin O_x$, which is used to delimit a local region centered at the pixel x. As done in [23], a Gaussian kernel function $G(x - y)$ is used as the indicator function of the local region O_x with the radius ρ, which is given by

$$G(z) = \begin{cases} \dfrac{1}{\alpha} e^{-|z|^2/2\sigma^2}, & |z| \le \rho \\ 0, & otherwise \end{cases} \tag{12}$$

with α being a constant such that $\int G(z)\mathrm{d}z = 1$ and σ being the standard deviation. It should be noted that the radius ρ should be chosen appropriately on the basis of the level of the intensity nonuniformity. The more inhomogeneous local intensity is, the faster bias field changes. In this case, a smaller value should be taken, and σ should also be smaller for the truncated Gaussian functions $G(z)$. Based on the indicator function of the local region, we can rewritten the local energy as

$$\varepsilon_x = \int_{\Omega} G(x - y) \left|u(y) - u_f(y)\right|^2 \mathrm{d}y \tag{13}$$

As described above, the intensity $u(y)$ in the local area O_x is separable, and thus can be divided into N categories by minimizing the local energy, which lead to the optimal partition of O_x with optimal cluster centers $(B(x)c_i + v(x))$. However, our final purpose is not to divide the neighborhood O_x, but to obtain an optimal partitions for the entire image region. This goal cannot be accomplished by minimizing a local energy ε_x for a point x. Minimization of ε_x for all the points x is necessary, which can be attained by minimizing the integral of ε_x over the entire image areas. Therefore, we defined an objective energy as following:

$$\varepsilon = \frac{1}{2} \iint_{\Omega} G(x - y) \left|u(y) - u_f(y)\right|^2 \mathrm{d}y\mathrm{d}x \tag{14}$$

C. LEVEL SET FORMULATION AND NUMERICAL IMPLEMENTATION

The objective energy defined by (14) is presented on the basis of partition $\left\{\Omega_j\right\}_{j=1}^N$. It is inconvenient to minimize the energy ε formulated by (14). In this section, we aim at converting the objective energy (14) to the level set formulation by utilizing one or multiple level set functions to represent the disjoint region and incorporating a length regularization term and a distance regularization term. The optimization of the energy can be implemented by solving the evolution equation of one or multiple level set functions.

1) TWO-PHASE SEGMENTATION

For the two-phase case, one level set function $\phi(x)$ is employed and the whole image domain is divided into two disjoint areas Ω_1 and Ω_2, which are the internal and external regions of the zero-level curve S. In this case, the local region-based fitting image defined in (9) can be expressed as

$$u_f(y) = \sum_{i=1}^{2} (B(x)c_i + v(x))\, M_i(\phi(y)), \quad y \in O_x \tag{15}$$

where $M_1(\phi) = H(\phi)$ and $M_2(\phi) = 1 - H(\phi)$. In numerical calculation, we substitute a regularized function H_ε given by $H_\varepsilon = \frac{1}{2}\left[1 + \frac{2}{\pi} arctan\left(\frac{x}{\varepsilon}\right)\right]$ for Heaviside function H, and accordingly the derivative of H_ε given by $\delta_\varepsilon = \frac{1}{\pi}\frac{\varepsilon}{\varepsilon^2+x^2}$ for the Dirac delta function δ.

The length regularization term $\mathcal{L}(\phi)$ is used in our model to punish the arc length of the zero-level curve, so the smoothness of the curve can be controlled by the parameter ν. In fact, the parameter ν has been discussed in previous studies [33], [34]. A big value of ν can be chosen to prevent some false outlines in the final segmentation results when segmenting the images corrupted by noise. A small value of ν can be taken to prevent the zero-level curve to cross boundaries or not to reach the desirable boundaries when dealing with the images with severe intensity nonuniformity and weak boundaries. Besides, in order to maintain the stability and accuracy of the level set, it is inevitable to guarantee the signed distance property $|\nabla\phi| = 1$ in the processing of the evolution. For this purpose, the penalty term $\Re(\phi)$ is introduced in our method. Therefore, by level set method, the total energy functional can be formulated as:

$$\begin{aligned} &F(\phi, c, B, \nu) \\ &= \frac{1}{2}\iint_\Omega G(x-y)\left|u(y) - u_f(y)\right|^2 \mathrm{d}y\mathrm{d}x \\ &\quad + \nu\int_\Omega |\nabla H(\phi(x))|\,\mathrm{d}x + \mu\int_\Omega \frac{1}{2}\left(|\nabla\phi(x)| - 1\right)^2 \mathrm{d}x \end{aligned} \tag{16}$$

The image segmentation result, the estimated bias field B and the local difference ν can be obtained by implementing the gradient descent method to optimize the total energy (16). The minimization is achieved through an iterative process. By variation method, the Gateaux derivative of the energy functional F can be calculated. Based on the theory that the function ϕ of minimizing the energy functional F satisfies the Euler Lagrange equation $\frac{\partial F}{\partial \phi} = 0$, the gradient flow equation i.e., the evolution equation of function ϕ, is presented by

$$\begin{aligned} \frac{\partial\phi}{\partial t} &= -\delta_\varepsilon(\phi(x))\int_\Omega G(x-y)[u(x) - u_f(x)]B(y)(c_2 - c_1)dy \\ &\quad + \nu\delta_\varepsilon div\left(\frac{\nabla\phi}{|\nabla\phi|}\right) + \mu\left(\nabla^2\phi - div\left(\frac{\nabla\phi}{|\nabla\phi|}\right)\right) \end{aligned} \tag{17}$$

with ∇ being the gradient operator, $div(\cdot)$ being the divergence operator. In our model, the level set evolution is implemented through the use of the explicit finite difference scheme [18]. The optimal c_i that minimizes the energy functional (16) for fixed $B(x)$, $\nu(x)$ and ϕ, is given by

$$c_i = \frac{\int (B * G)\, uM_i dy - \int (B\nu * G)\, M_i dy}{\int \left(B^2 * G\right) M_i dy} \tag{18}$$

Keeping c, $\nu(x)$, and ϕ fixed, the optimal $B(x)$ that minimizes $F(\phi, c, B, \nu)$, is given by

$$B(x) = \frac{G * \left(u\sum_{i=1}^{2} c_i M_i\right) - \nu(x)\left(G * \sum_{i=1}^{2} c_i M_i\right)}{G * \sum_{i=1}^{2} c_i^2 M_i} \tag{19}$$

Keeping c, $B(x)$, and ϕ fixed, the optimal $\nu(x)$ that minimizes $F(\phi, c, B, \nu)$, is given by

$$\nu(x) = \frac{G * u - B(x)\left(G * \sum_{i=1}^{2} c_i M_i\right)}{G * 1} \tag{20}$$

2) MULTIPHASE SEGMENTATION

For the case of $N \geq 3$, the whole image domain is divided into three or more disjoint areas Two or more level set functions $\{\phi_i\}_{i=1}^n$ are employed to distinguish areas $\{\Omega_i\}_{i=1}^N$ The membership function of the region Ω_i is formulated as

$$M_i(\phi_1(x), \phi_2(x), \cdots, \phi_n(x)) = \begin{cases} 1 & x \in \Omega_i \\ 0 & \text{otherwise} \end{cases} \tag{21}$$

For convenience, we denote $\Phi = (\phi_1, \phi_2, \cdots, \phi_n)$. For the case of N = 3 and N = 4, we use two level set functions $\phi_1(x)$ and $\phi_2(x)$ to define the corresponding membership functions. The membership functions in the three-phase case can be written as

$$\begin{aligned} M_1(\Phi) &= H_\varepsilon(\phi_1)H_\varepsilon(\phi_2) \\ M_2(\Phi) &= H_\varepsilon(\phi_1)\left(1 - H_\varepsilon(\phi_2)\right) \\ M_3(\Phi) &= 1 - H_\varepsilon(\phi_1) \end{aligned} \tag{22}$$

For the case of $N = 4$, the definition of $M_i(\phi)$ can be expressed as

$$\begin{aligned} M_1(\Phi) &= H_\varepsilon(\phi_1)H_\varepsilon(\phi_2) \\ M_2(\Phi) &= H_\varepsilon(\phi_1)\left(1 - H_\varepsilon(\phi_2)\right) \\ M_3(\Phi) &= \left(1 - H_\varepsilon(\phi_1)\right)H_\varepsilon(\phi_2) \\ M_4(\Phi) &= \left(1 - H_\varepsilon(\phi_1)\right)\left(1 - H_\varepsilon(\phi_2)\right) \end{aligned} \tag{23}$$

We use the three-phase segmentation model to segment the normal brain Magnetic Resonance (MR) images in this paper. In this case, the local region-based fitting image defined in (9) can be formulated as:

$$u_f(y) = \sum_{i=1}^{3}\left(B(x)c_i + \nu(x)\right)M_i(\Phi(y)),\ y \in O_x \tag{24}$$

The total energy of the three-phase level set formation is expressed as

$$\begin{aligned} F(\Phi, c, B, \nu) &= \frac{1}{2}\iint_\Omega G(x-y)\left|u(y) - u_f(y)\right|^2 \mathrm{d}y\mathrm{d}x \\ &\quad + \nu\sum_{i=1}^{2}\int_\Omega |\nabla H(\phi_i(x))|\,\mathrm{d}x \\ &\quad + \mu\sum_{i=1}^{2}\int_\Omega \frac{1}{2}\left(|\nabla\phi_i(x)| - 1\right)^2 \mathrm{d}x \end{aligned} \tag{25}$$

Keeping c, $B(x)$ and $\nu(x)$ fixed, the minimization of $F(\Phi, c, B, \nu)$ with respect to Φ can be implemented by solving the following gradient flow equations:

$$\frac{\partial\phi_1}{\partial t} = -\gamma_1\int_\Omega G(x-y)[u(x) - u_f(x)]B(y)dy$$

$$+\nu\delta_\varepsilon div\left(\frac{\nabla\phi_1}{|\nabla\phi_1|}\right)+\mu\left(\nabla^2\phi_1-div\left(\frac{\nabla\phi_1}{|\nabla\phi_1|}\right)\right) \tag{26}$$

$$\frac{\partial\phi_2}{\partial t}=-\gamma_2\int_\Omega G(x-y)[u(x)-u_f(x)]B(y)dy +\nu\delta_\varepsilon div\left(\frac{\nabla\phi_2}{|\nabla\phi_2|}\right)+\mu\left(\nabla^2\phi_2-div\left(\frac{\nabla\phi_2}{|\nabla\phi_2|}\right)\right) \tag{27}$$

with

$$\begin{aligned}\gamma_1&=\delta_\varepsilon(\phi_1)[(c_2-c_1)H_\varepsilon(\phi_2)+c_3-c_2]\\ \gamma_2&=\delta_\varepsilon(\phi_2)(c_2-c_1)H_\varepsilon(\phi_1)\end{aligned} \tag{28}$$

We can minimize the energy functional (25) by the identical procedure with that of the two-phase case. And the optimal c, $B(x)$ and $v(x)$ that minimize the energy (25) can be calculated as follows, respectively:

$$c_i=\frac{\int(B*G)\,uM_idy-\int(Bv*G)\,M_idy}{\int\left(B^2*G\right)M_idy} \tag{29}$$

$$B(x)=\frac{G*\left(u\sum_{i=1}^{3}c_iM_i\right)-v(x)\left(G*\sum_{i=1}^{3}c_iM_i\right)}{G*\sum_{i=1}^{3}c_i^2M_i} \tag{30}$$

$$v(x)=\frac{G*u-B(x)\left(G*\sum_{i=1}^{3}c_iM_i\right)}{G*1} \tag{31}$$

IV. EXPERIMENTAL RESULTS AND DISCUSSION

In this section, our model is evaluated on synthetic images and real images with different degree of intensity nonuniformity. All the experiments have been carried out with MATLAB2011b on the PC with an Intel (R) Core (TM) 2.70 GHz CPU, 4 GB RAM and Windows 7 64-bit. Unless otherwise specified, we set the parameter as follow:$\sigma=3$, $\varepsilon=1$, time step $\Delta t=0.025$ and $\mu=1$. For fair comparison, all best parameters are selected for the other models. Besides visual evaluation, the performance of our model and the other models also are compared quantitatively by the Dice coefficient (DC) [21], [32], the Jaccard similarity (JS) [21], the false positive (FPF) and false negative fraction (FNF) [29]. These metrics are written as:

$$JS=\frac{N(A_1\cap A_2)}{N(A_1\cup A_2)},\quad ,DC=\frac{2N(A_1\cap A_2)}{N(A_1)+N(A_2)},$$
$$FPF=\frac{N(A_1\backslash O)}{N(A_1)},\quad FNF=\frac{N(A_2\backslash O)}{N(A_2)},$$

where A_1 stands for the foreground of the ground truth image, A_2 indicates the foreground from the test model, O represents the common region of A_1 and A_2, and $N(\cdot)$ is the pixel numbers of the region. The closer the values of JS and DC are to 1, and the values of FPF and FNF are to 0, the more accurate the experimental results of the models are.

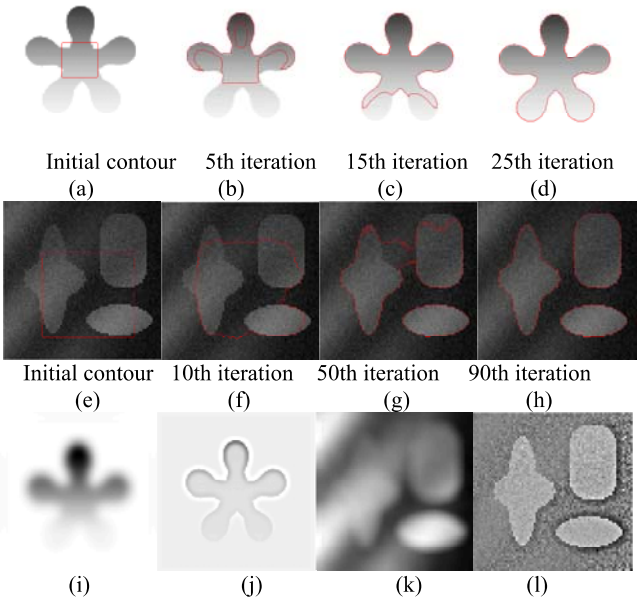

FIGURE 1. Segmentation processes and results of our model: (a), (e): the input images and the initial contours represented by red solid lines. (b), (c), (f), (g): the evolutionary process of the zero-level contour. (d), (h): the results of our model. (i), (k): the estimated bias fields from our model. (j), (l): the bias corrected images from our model.

A. TWO PHASE SEGMENTATION

Fig. 1 illustrates the evolutionary process of the zero-level contour and the segmentation results from our model on two synthetic images corrupted by intensity nonuniformity. In this experiment, the length term coefficient ν of our model are chosen to be $0.001\times255\times255$ and $0.003\times255\times255$, respectively. Fig. 1(a) and (e) are the input images and the initial zero-level contours represented by red solid lines. Fig. 1(b), (c), (f) and (g) illustrate the evolutionary process of the zero-level set. Fig. 1(d) and (h) are the results of our model. Fig. 1(i) and (k) are the estimated bias fields from our model. Fig. 1(j) and (l) are the bias corrected images from our model. The results indicate that our model achieves desirable results due to exploiting local region information, which can separate the objects from its background in images with intensity nonuniformity.

Fig. 2 shows the robustness of our model to initial curve location. Our model is used to segment two synthetic images under four different initializations. The values of ν in our model for the two images are $0.003\times255\times255$ and $0.0005\times255\times255$, respectively. The first synthetic image is the same as the second one in Fig. 1. Row 1 and 3 show four different initializations of the zero-level function on the two synthetic images. We exhibit the corresponding results of our method in row 2 and 4, respectively. Although these initial locations are quite different, our model can get almost the same results, which correctly capture the boundaries. It is clear that our method can achieve desirable segmentation results with different locations of the initial curve, which testify the robustness of our model to the initial curve location.

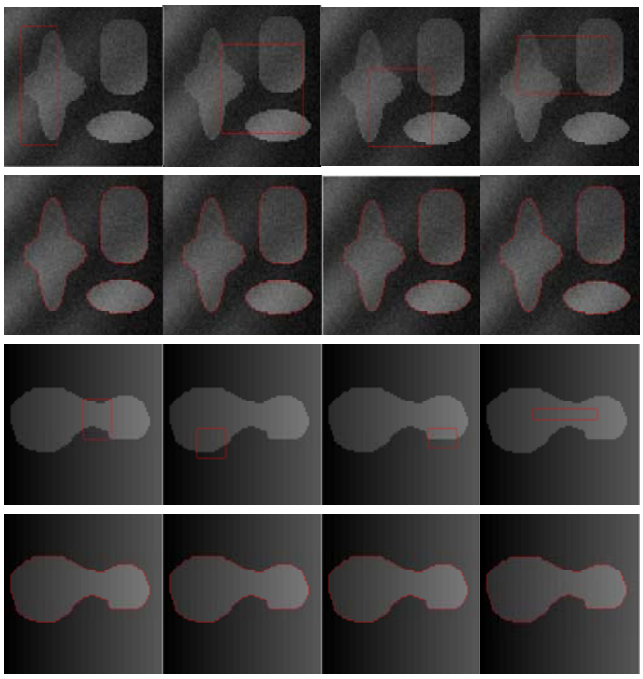

FIGURE 2. Segmentation results on two synthetic images under four different initializations. Row 1 and row 3: four different initializations. Row 2 and row 4: the corresponding segmentation results.

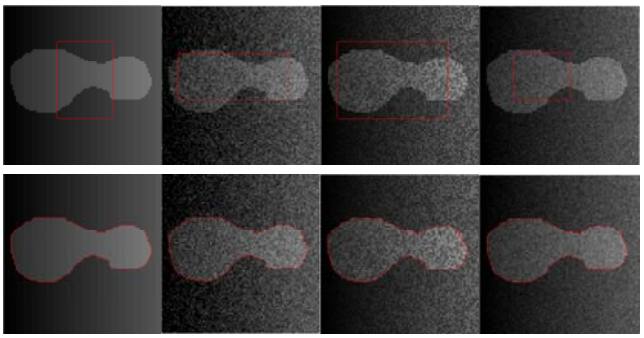

FIGURE 3. Segmentation results of noise and noise-free images. Row 1: original and three kinds of noise images. Row 2: the corresponding segmentation results.

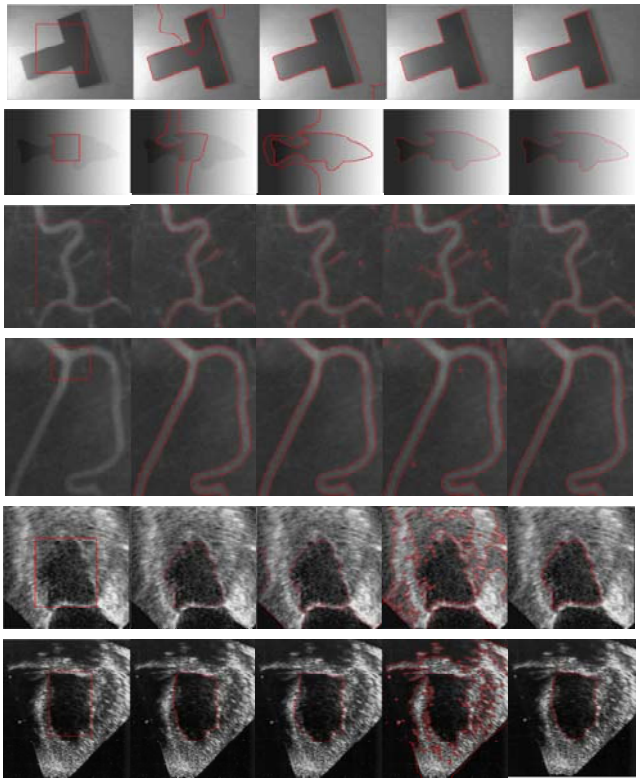

FIGURE 4. Comparison of our method with LBF, MLIC, LSM. Column 1: the input images and the initialization. Column 2 to 5: the results using LBF, MLIC, LSM, and our method, respectively.

Fig. 3 shows that our method can deal with images polluted by noisy. The first image in row 1 is a noise-free image, and the other three images in row 1 are three kinds of noise images created by adding noise to the noise-free image. These three noise images are obtained by using the MATLAB function "*imnoise*" to add Gaussian noise with zero mean and 0.003 variance, speckle noise with zero mean and 0.003 variance, passion noise with default parameters of the MATLAB "*imnoise*" function to the first image in row 1, respectively. Row 2 represent the segmentation results accordingly. The coefficients ν of length regularization term in our model for three kinds of noise images are set to be $0.01\times255\times255$, $0.03\times255\times255$ and $0.3\times255\times255$, respectively. It is easy to see that our method can handle different kind of noise images and can segment images accurately in the presence of noise and intensity nonuniformity.

Fig. 4 shows the comparison results of our model with LBF, MLIC, and LSM on four medical images and two synthetic images with intensity nonuniformity. The values of ν in our model for the images are $0.003 \times 255 \times 255$, $0.0001 \times 255 \times 255$, $0.0015 \times 255 \times 255$, $0.0015 \times 255 \times 255$, $0.05 \times 255 \times 255$ and $0.05 \times 255 \times 255$, respectively. The input images and the initial contours are shown in column 1. The segmentation results of LBF, MLIC, LSM and our method are shown in column 2 to 5, respectively. Because our model utilizes the bias field and the intensity information and simultaneously considers the difference matrix between the input image and estimated image, it achieves better results in handling intensity nonuniformity. Although LBF works well in segmenting the first synthetic image, it failed to segment the second image. LSM is just the opposite. When LSM is used to segment the four medical images, even though we have done our best to adjust the parameters, the result of LSM model is not satisfactory. Although the segmentation result of LBF model on four medical images is better than that of MLIC and LSM, LBF model has strict requirement for the position of the initial curve, and therefore when the initialization curve is set improperly, it could not get accurate segmentation results. From the experimental results, it is clear that our model has a better performance in segmenting images with intensity nonuniformity.

TABLE 1. Cpu time and iteration of our method compared with the state-of-the-art methods.

Img	Size	LBF [16]		MLIC [29]		LIC [23]		Our mode	
		CPU time (s)	Iteration	CPU time (s)	Iteration	CPU time (s)	Iteration	CPU time (s)	Iteration
1	127*319	1.0296	36	2.0436	32	1.2324	38	0.9828	14
2	96*127	0.8736	93	4.0404	138	1.6224	126	0.6084	12
3	85*88	0.2184	22	0.6396	41	0.5928	56	0.1716	9

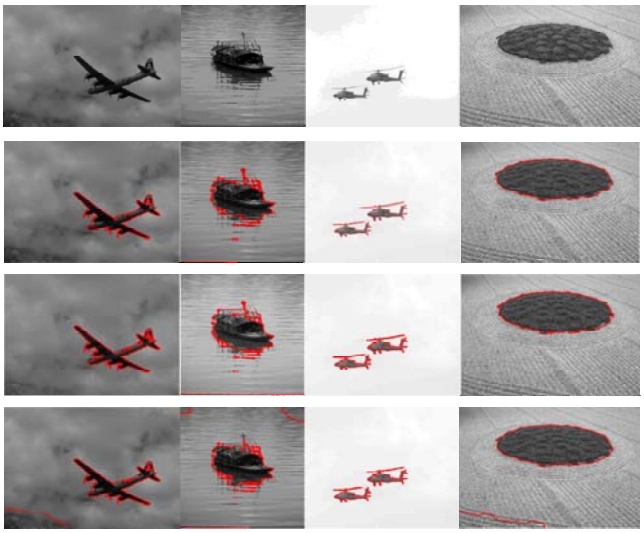

FIGURE 5. Comparison of our method with LHIF and MLIC. Row 1: the input images. Row 2 to 4: the results using our model, LHIF and MLIC, respectively.

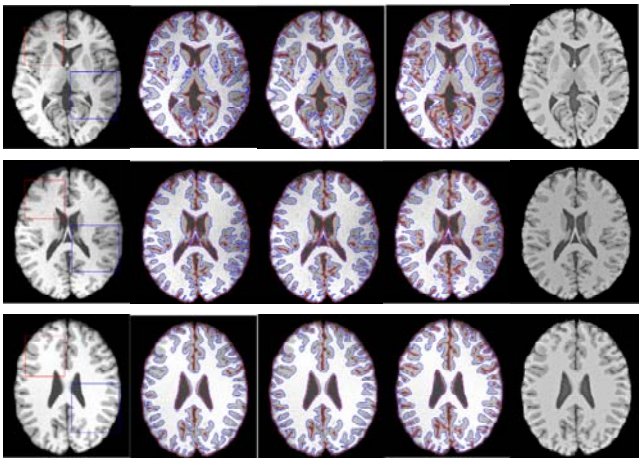

FIGURE 7. Comparison results of our model with LIC and MLIC on three brain MRI images with different degrees of intensity nonuniformity. Column 1: three input brain MRI images and the initializations. Column 2 to 4: the results of LIC, MLIC and our model. Column 5: the bias corrected images from our model.

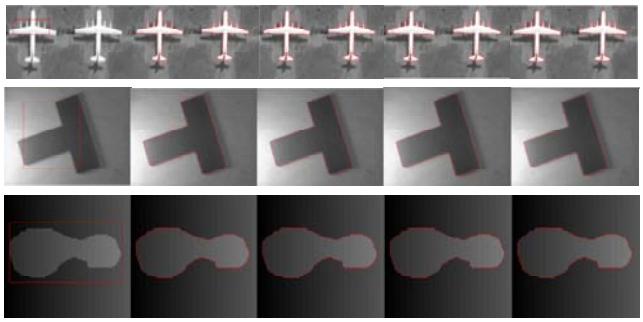

FIGURE 6. Segmentation results and the initialization. Column 1: three images with the initializations. Column 2 to 4: the segmentation results of LBF, MLIC, LIC, and our method, respectively.

Fig. 5 shows the comparison results of our model with LHIF and MLIC on four real images containing intensity nonuniformity. The values of ν in our model for the four images are $0.003 \times 255 \times 255$, $0.03 \times 255 \times 255$, $0.001 \times 255 \times 255$ and $0.03 \times 255 \times 255$, respectively. The input images are shown in row 1. The segmentation results of our method, LHIF and MLIC are shown in row 2 to 4, respectively. For the sake of fair comparison, we set desirable parameters for LHIF and MLIC. It is can be seen that our model can get desirable segmentation results. The LHIF model can deal with images with strong intensity nonuniformity, but it does not perform well at the images with weak boundaries. The MLIC model is just the opposite. Duo to the local region-based fitting image, our model can fit the image intensity well and deal with strong intensity nonuniformity and weak boundaries.

In this experiment, we compare the execution time of our model with LBF, MLIC and LIC. For this purpose, we apply LBF, MLIC, LIC and our model to segment three images with intensity nonuniformity. The segmentation results of this experiment are exhibited in Fig. 6. The values of ν in our model for the three images are $0.01 \times 255 \times 255$, $0.003 \times 255 \times 255$ and $0.001 \times 255 \times 255$, respectively. Column 1 exhibits three images and the initializations. Column 2 to 5 display the experimental results of LBF, MLIC, LIC and our model, respectively. For fair comparison, we carefully chose the common initialization location suitable for each model to obtain desirable results and selected the optimal parameters for the other models. The CPU time and iteration numbers of these models in Table 1 indicate that our method takes less CPU time than the other three methods to segment the three images.

B. MULTIPHASE SEGMENTATION

In this experiment, we apply three-phase model of our method to segment three brain MR images and compare with LIC and

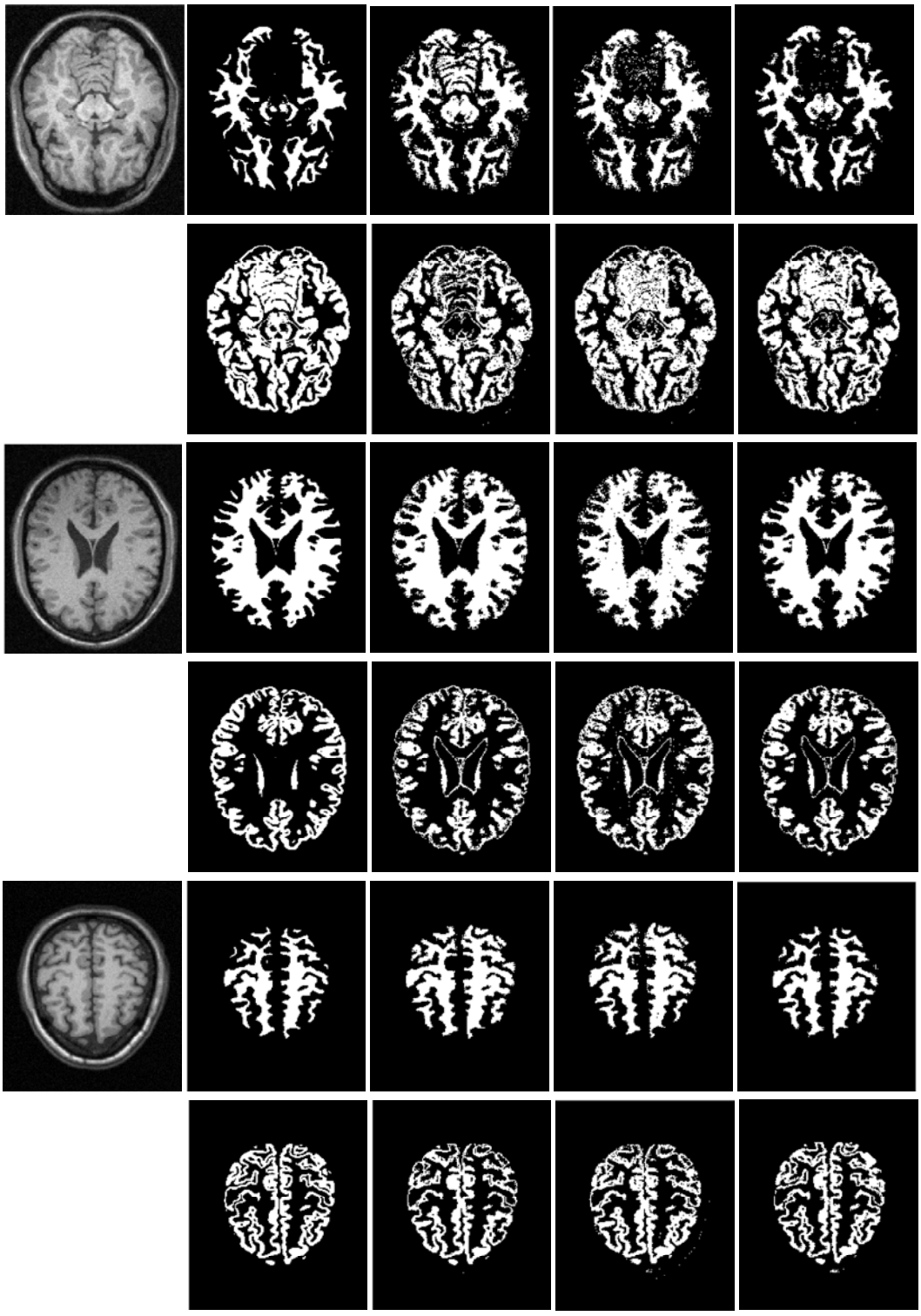

FIGURE 8. Comparison results of our method with LIC and MICO on three brain MR images. Row 1, 3 and 5: WM. Row 2, 4 and 6: GM. All WM and GM are shown in white. Column 1: three simulated MR images. Column 2 to 5: the ground truth and the segmentation results of LIC, MICO and our method, respectively.

MLIC. These brain images are divided into three parts: white matter (WM), gray matter (GM) and background, which includes cerebrospinal fluid (CSF). We set ν =0.005 $\times$ 255 $\times$ 255, $\varepsilon = 1.5$, $\sigma = 4$ and time step $\Delta t = 0.1$ for our model. Three brain MR images with the initializations are exhibited in column 1 of Fig. 7. The experimental results of LIC, MLIC

TABLE 2. Performance evaluations of white matter and gray matter segmentation quality between different methods.

	White matter			Gray matter		
	MICO [30]	LIC [23]	Our model	MICO [30]	LIC [23]	Our model
JS	0.81 ±0.04	0.81 ± 0.06	0.83 ±0.04	0.70 ±0.03	0.71 ± 0.03	0.74 ± 0.02
DSC	0.89 ± 0.03	0.89 ± 0.04	0.91 ± 0.02	0.83 ± 0.02	0.83 ± 0.02	0.85 ± 0.01
FPF	0.06 ± 0.01	0.05 ± 0.01	0.08 ± 0.02	0.18 ± 0.03	0.19± 0.04	0.15 ± 0.02
FNF	0.15 ± 0.04	0.16 ± 0.06	0.10 ± 0.03	0.17 ± 0.02	0.15 ± 0.02	0.14 ± 0.02

and our model are exhibited in column 2 to 5, respectively. The bias corrected images from our model are displayed in the last column. Fig. 7 show that our method can detect more CSF than LIC and MLIC in segmenting these three images, and our model can capture more GM than LIC and MLIC in segmenting the first images. The incorporation of the local region-based fitting in our model makes our model better than the other two models.

In this experiment, the experimental results of our method are evaluated and compared with that of LIC and MICO. More than 100 simulated brain MR images are used in the experiment. These images with the ground truth were obtained from *BrainWeb* (http://www.bic.mni.mcgill.ca/brainweb/). All of images were corrupted with bias field and noise. We chose three of them to be shown in Figure 8. We set $\nu = 0.005 \times 255 \times 255$, $\varepsilon = 1.5$, $\sigma = 4$ and time step $\Delta t = 0.06$ for all images in this test. Figure 8 shows comparison results of our method with LIC and MICO. Column 1 are three brain MR images. The ground truth and the experimental results of LIC, MICO and our method, are displayed in column 2 to 5, respectively. Row 1, 3 and 5 are GM and row2, 4 and 6 are WM. All WM and GM are shown in white. Because our model uses the information of bias field and the intensity, and simultaneously takes into account the difference between the input image and estimated image to approximate the image intensity, it can get more accurate results of segmentation. As shown in Fig. 8, our method can detect more GM than LIC and MICO in segmenting these images. In other words, over-segmentation of WM occurred in LIC model and MICO model. The average JS values, DSC values, FPF values and FNF values for the GM and WM gained from the three models are exhibited in Table 2, which demonstrates that our method has achieved a better performance in segmenting these images. It should be noted that the average value of FPF of our model is higher and at the same time a lower FNF value than that of the other two models due to the over-segmentation of WM in LIC model and MICO model.

V. CONCLUSION

We have proposed an active contour model based on local intensity fitting energy for segmentation and nonuniformity correction of images. Based on an improved image model incorporating the bias field, the bias-free image intensity and local difference matrix, the local region-based fitting image is introduced in our framework. An energy functional is defined by minimizing the difference between the local region-based fitting image and the input image in the local area around each pixel. By variational level set method, this energy is combined with two regularization terms to build up the total energy. Experimental results on synthetic images and real images as well as comparison with state of-the-art models have shown that our method is robust to the initial curve location and noise, and offers significant improvements in both accuracy and execution time.

REFERENCES

[1] W. Li, Y. Wang, J. Du, and J. Lai, "Synergistic integration of graph-cut and cloud model strategies for image segmentation," *Neurocomputing*, vol. 257, pp. 37–46, Sep. 2017.

[2] T. Lei, X. Jia, Y. Zhang, L. He, H. Meng, and A. K. Nandi, "Significantly fast and robust fuzzy C-means clustering algorithm based on morphological reconstruction and membership filtering," *IEEE Trans. Fuzzy Syst.*, to be published, doi: 10.1109/TFUZZ.2018.2796074.

[3] M. Gong, H. Li, X. Zhang, Q. Zhao, and B. Wang, "Nonparametric statistical active contour based on inclusion degree of fuzzy sets," *IEEE Trans. Fuzzy Syst.*, vol. 24, no. 5, pp. 1176–1192, Oct. 2016.

[4] C. G. Bampis, P. Maragos, and A. C. Bovik, "Graph-driven diffusion and random walk schemes for image segmentation," *IEEE Trans. Image Process.*, vol. 26, no. 1, pp. 35–50, Jan. 2017.

[5] C. Scharfenberger, A. G. Chung, A. Wong, and D. A. Clausi, "Salient region detection using self-guided statistical non-redundancy in natural images," *IEEE Access*, vol. 4, pp. 48–60, Nov. 2015.

[6] C. R. Meyer, P. H. Bland, and J. Pipe, "Retrospective correction of intensity inhomogeneities in MRI," *IEEE Trans. Med. Imag.*, vol. 14, no. 1, pp. 36–41, Mar. 1995.

[7] Y. Chen, J. Zhang, and J. Yang, "An anisotropic images segmentation and bias correction method," *Magn. Reson. Imag.*, vol. 30, no. 1, pp. 85–95, Jan. 2012.

[8] M. Styner, C. Brechbuhler, G. Szckely, and G. Gerig, "Parametric estimate of intensity inhomogeneities applied to MRI," *IEEE Trans. Med. Imag.*, vol. 19, no. 3, pp. 153–165, Mar. 2000.

[9] T. F. Chan and L. A. Vese, "Active contour without edges," *IEEE Trans. Image Process.*, vol. 10, no. 2, pp. 266–277, Feb. 2001.

[10] Y. Zhou *et al.*, "Active contours driven by localizing region and edge-based intensity fitting energy with application to segmentation of the left ventricle in cardiac CT images," *Neurocomputing*, vol. 156, pp. 199–210, May 2015.

[11] N. Paragios and R. Deriche, "Geodesic active contours and level sets for the detection and tracking of moving objects," *IEEE Trans. Pattern Anal. Mach. Intell.*, vol. 22, no. 3, pp. 266–280, Mar. 2000.

[12] B. N. Li, J. Qin, R. Wang, M. Wang, and X. Li, "Selective level set segmentation using fuzzy region competition," *IEEE Access*, vol. 4, pp. 4777–4788, Aug. 2016.

[13] J. Lie, M. Lysaker, and X.-C. Tai, "A binary level set model and some applications to Mumford-Shah image segmentation," *IEEE Trans. Image Process.*, vol. 15, no. 5, pp. 1171–1181, May 2006.

[14] H. Lv, Z. Wang, S. Fu, C. Zhang, L. Zhai, and X. Liu, "A robust active contour segmentation based on fractional-order differentiation and fuzzy energy," *IEEE Access*, vol. 5, pp. 7753–7761, Apr. 2017.

[15] K. Zhang, H. Song, and L. Zhang, "Active contours driven by local image fitting energy," *Pattern Recognit.*, vol. 43, no. 4, pp. 1199–1206, Apr. 2010.

[16] C. Li, C.-Y. Kao, J. C. Gore, and Z. Ding, "Implicit active contours driven by local binary fitting energy," in *Proc. IEEE Conf. Comput. Vis. Pattern Recognit.*, Minneapolis, MN, USA, Jun. 2007, pp. 1–7.

[17] C. Li, C.-Y. Kao, J. C. Gore, and Z. Ding, "Minimization of region-scalable fitting energy for image segmentation," *IEEE Trans. Image Process.*, vol. 17, no. 10, pp. 1940–1949, Oct. 2008.

[18] C. Li, C. Xu, C. Gui, and M. D. Fox, "Level set evolution without re-initialization: A new variational formulation," in *Proc. IEEE Conf. Comput. Vis. Pattern Recognit.*, Jun. 2005, pp. 430–436.

[19] B. Wang, X. Gao, D. Tao, and X. Li, "A nonlinear adaptive level set for image segmentation," *IEEE Trans. Cybern.*, vol. 44, no. 3, pp. 418–429, Mar. 2013.

[20] A. Khadidos, V. Sanchez, and C.-T. Li, "Weighted level set evolution based on local edge features for medical image segmentation," *IEEE Trans. Image Process.*, vol. 26, no. 4, pp. 1979–1991, Apr. 2017.

[21] C. Liu, W. Liu, and W. Xing, "An improved edge-based level set method combining local regional fitting information for noisy image segmentation," *Signal Process.*, vol. 130, pp. 12–21, Jan. 2017.

[22] V. Caselles, R. Kimmel, and G. Sapiro, "Geodesic active contours," in *Proc. IEEE Conf. Comput. Vis. Pattern Recognit.*, Cambridge, MA, USA, Jun. 1995, pp. 61–79.

[23] C. Li, R. Huang, Z. Ding, J. C. Gatenby, D. N. Metaxas, and J. C. Gore, "A level set method for image segmentation in the presence of intensity inhomogeneities with application to MRI," *IEEE Trans. Image Process.*, vol. 20, no. 7, pp. 2007–2016, Jul. 2011.

[24] X.-F. Wang, H. Min, L. Zou, and Y.-G. Zhang, "A novel level set method for image segmentation by incorporating local statistical analysis and global similarity measurement," *Pattern Recognit.*, vol. 48, no. 1, pp. 189–204, 2015.

[25] K. Zhang, L. Zhang, K.-M. Lam, and D. Zhang, "A level set approach to image segmentation with intensity inhomogeneity," *IEEE Trans. Cybern.*, vol. 46, no. 2, pp. 546–557, Feb. 2016.

[26] T. Zhan, J. Zhang, L. Xiao, Y. Chen, and Z. Wei, "An improved variational level set method for MR image segmentation and bias field correction," *Magn. Reson. Imag.*, vol. 31, no. 3, pp. 439–447, Apr. 2013.

[27] C. He, Y. Wang, and Q. Chen, "Active contours driven by weighted region-scalable fitting energy based on local entropy," *Signal Process.*, vol. 92, no. 2, pp. 587–600, Feb. 2012.

[28] S. Niu, Q. Chen, L. de Sisternes, Z. Ji, Z. Zhou, and D. L. Rubin, "Robust noise region-based active contour model via local similarity factor for image segmentation," *Pattern Recognit.*, vol. 61, pp. 104–119, Jan. 2017.

[29] C. Huang and L. Zeng, "An active contour model for the segmentation of images with intensity inhomogeneities and bias field estimation," *PLoS ONE*, vol. 10, no. 4, pp. 1–24, Apr. 2015.

[30] C. Li, J. C. Gore, and C. Davatzikos, "Multiplicative intrinsic component optimization (MICO) for MRI bias field estimation and tissue segmentation," *Magn. Reson. Imag.*, vol. 32, no. 7, pp. 913–923, Sep. 2014.

[31] Y. Chen, X. Yue, R. Y. Da Xu, and H. Fujita, "Region scalable active contour model with global constraint," *Knowl.-Based Syst.*, vol. 120, pp. 57–73, Mar. 2017.

[32] L. Wang, Y. Chang, H. Wang, Z. Wu, J. Pu, and X. Yang, "An active contour model based on local fitted images for image segmentation," *Inf. Sci.*, vol. 418, pp. 61–73, Mar. 2017.

[33] M. Li, C. He, and Y. Zhan, "Adaptive regularized level set method for weak boundary object segmentation," *Math. Problems Eng.*, vol. 2012, Feb. 2012, Art. no. 369472.

[34] L. Wang, J. Zhu, M. Sheng, A. Cribb, S. Zhu, and J. Pu, "Simultaneous segmentation and bias field estimation using local fitted images," *Pattern Recognit.*, vol. 74, pp. 145–155, Feb. 2018.

[35] K. Ding, L. Xiao, and G. Weng, "Active contours driven by local pre-fitting energy for fast image segmentation," *Pattern Recogn. Lett.*, vol. 104, no. 1, pp. 29–36, Mar. 2018.

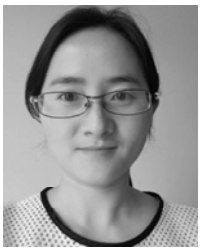

XIAOYING SHAN received the B.S. and M.S. degrees from the School of Mathematics and Applied Mathematics, Zhengzhou University, Zhengzhou, China, in 2005 and 2008, respectively. She is currently pursuing the Ph.D. degree with the College of Electronic and Information Engineering, Tongji University, Shanghai, China. Her research interests include medical image processing and computer vision.

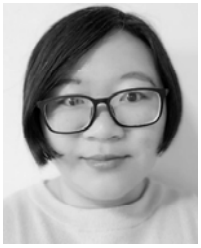

XIAOLIANG GONG received the Ph.D. degree in physics from East China Normal University in 2012. She is currently an Engineer with the College of Electronic and Information Engineering, Tongji University, Shanghai, China. Her research topics are in biological signal processing, including ECG, EEG, and MRI.

ASOKE K. NANDI received the Ph.D. degree from the University of Cambridge (Trinity College), Cambridge, U.K. In 1983, he co-discovered three fundamental particles known as W^+, W^-, and Z (the UA1 team at CERN), providing the evidence for the unification of the electromagnetic and weak forces, which was recognized by the Nobel Committee for Physics in 1984. He held academic positions at several universities, including Oxford University, U.K.; Imperial College London, U.K.; The University of Strathclyde, U.K.; and the University of Liverpool, U.K. In 2013, he moved to Brunel University, London, U.K., where he was the Chair and the Head of electronic and computer engineering. He is a Distinguished Visiting Professor at Tongji University, Shanghai, China, and an Adjunct Professor with the University of Calgary, Calgary, AB, Canada.

He has authored over 550 technical publications, including 220 journal papers and four books *Automatic Modulation Classification: Principles, Algorithms and Applications* (Wiley, 2015), *Integrative Cluster Analysis in Bioinformatics* (Wiley, 2015), *Blind Estimation Using Higher- Order Statistics* (Springer, 1999), and *Automatic Modulation Recognition of Communications Signals* (Springer, 1996). The h-index of his publications is 67 (Google Scholar) and ERDOS number is 2. His current research interests lie in the areas of signal processing and machine learning, with applications to communications, gene expression data, functional magnetic resonance data, and biomedical data. He has made many fundamental theoretical and algorithmic contributions to many aspects of signal processing and machine learning. He has much expertise in big data, dealing with heterogeneous data, and extracting information from multiple data sets obtained in different laboratories and different times.

Dr. Nandi is a fellow of the Royal Academy of Engineering and seven other institutions. Among the many awards he received are the Mountbatten Premium Division Award from the Electronics and Communications Division, Institution of Electrical Engineers, in 1998, the Water Arbitration Prize from the Institution of Mechanical Engineers, U.K., in 1999, the Glory of Bengal Award for his outstanding achievements in scientific research in 2010, and the IEEE Heinrich Hertz Award in USA in 2012. He is an IEEE Distinguished Lecturer with the EMBS Society (2018–2019).